# Space-Variant and Anisotropic Resolution Modeling in List-Mode EM Reconstruction

Arman Rahmim, Mark Lenox, Christian Michel, Andrew J. Reader, and Vesna Sossi

***Abstract*— One issue common to PET scanners is the *space-variance* of the point spread function (PSF): manifesting itself as resolution degradation as one moves away from the center of the field-of-view (FOV). This effect occurs due to a higher probability of inter-crystal penetration with higher angles of radiation incident on crystal fronts. Depth-of-interaction (DOI) encoding is known to improve this problem, but has not reached complete space-invariance. In this work, a space-variant PSF has been incorporated into the system matrix of a list-mode EM algorithm. Furthermore, in an effort to further extend generality and accuracy of the model, *anisotropicity* of the PSF has also been considered: finite resolution effects at any position in the FOV are allowed to have distinct values along the axial and the two transaxial directions, and are allowed to degrade differently with increasing distance from the center of the FOV. The spatial distribution of image resolution has been measured and fit using exponential and inverse-Gaussian functions. It is shown that the proposed modeling of the PSF, compared to space-invariant and isotropic modeling, improves resolution recovery across the FOV.**

## I. Introduction

One of the key motivations behind the wide-spread use of iterative techniques over analytical methods has been the ability to incorporate more accurate modeling of system response in the PET acquisition process. In expectation maximization (EM) algorithms, the system matrix may be utilized to incorporate finite resolution effects, such as the *space-variance* of the point spread function (PSF): degradation in resolution of imaged point sources as one moves away from the center of the field-of-view (FOV) [1]. This effect is mainly caused by the dependence of inter-crystal penetration on angle of incidence of radiation [2]. As radiation occurs in voxels increasingly distant from the center of the FOV, it is more likely for the radiation to reach crystal fronts at higher angles of incidence, and to subsequently penetrate and be recorded in nearby crystals, ultimately degrading image resolution for such voxels (commonly referred to as the *parallax* effect).

Measurement of depth-of-interaction (DOI) within the crystals is known to minimize this problem, but its implementation has not achieved complete spatial invariance for resolution (see for e.g. [3]). A space-variant penalty term in penalized-likelihood reconstruction has been previously utilized to model space-variance in system response [4], [5]. In expectation maximization (EM) algorithms, the system matrix may be utilized to incorporate space-variance of the system, as elaborated later.

Furthermore, spatial resolution for various scanners is commonly reported in the literature to be *anisotropic* (i.e. the PSF at a given position in the FOV exhibits distinct values along the axial and the two transaxial directions). This should be critical in correct modeling of the parallax effect, which exhibits anisotropic resolution at positions away from the center of the FOV. To our knowledge, an actual attempt at appropriately incorporating space-variance along with anisotropicity of the PSF has not been previously made. Simultaneous modeling of these two factors can allow more accurate characterization of degradation of each of the axial and the two transaxial resolution widths as one moves away from the center of the FOV.

In this work, we have used code parallelization to achieve an efficient implementation of system response PSF space-variance and anisotropicity using the system matrix formulation. The corresponding theory is described in Sec. II, with further elaboration on measurement of finite resolution kernels in Sec. III. The experimental procedure along with preliminary results of implementation of the aforementioned modeling are described in sections IV and V.

## II. Modeling of Space-Variance and Anisotropicity

In what follows, we describe how modeling of image resolution may be incorporated into the list-mode EM reconstruction technique. Since modeling is included into the system matrix, which is similarly utilized in histogram-mode EM reconstruction, extension of such space-variant and/or anisotropic modeling to histogram-mode EM algorithm is straightforward, as pursued in [6] with space-invariant and isotropic resolution kernels.

Denoting $\lambda_j^m$ as the image intensity in voxel $j$ ($j$=1...$J$) at the $m$th iteration, and $p_{ij}$ as the probability of an emission from voxel $j$ being detected along LOR $i$, the list-mode expectation maximization (LM-EM) reconstruction algorithm is given by [7]

$$\lambda_j^{m+1} = \frac{\lambda_j^m}{s_j} \sum_{k=1}^{N} p_{i_k j} \frac{1}{\sum_{a=1}^{J} p_{i_k a} \lambda_a^m} \qquad (1)$$

where $i_k$ refers to the LOR along which the $k$th list-mode event is detected, $N$ is the number of measured events, and

Manuscript received October 29, 2003.

Arman Rahmim and Vesna Sossi are with the Department of Physics and Astronomy, University of British Columbia, Vancouver, BC Canada (email rahmim@physics.ubc.ca,vesna@physics.ubc.ca)

Mark Lenox and Christian Michel are with CPS Innovations, Knoxville, TN USA (email Mark.Lenox@cpspet.com, Christian.Michel@cpspet.com).

Andrew J. Reader is with the Department of Instrumentation and Analytical Science UMIST, Manchester, UK (email andrew.j.reader@umist.ac.uk).

0-7803-8257-9/04/$20.00 © 2004 IEEE.

the sensitivity correction factor $s_j$=$\sum_{i=1}^{I} p_{ij}$ is a summation over all possible measurable LORs ($i$=1...$I$)

We next note that, following the approach of Ref. [8], the system matrix or operator $\hat{P}$=$(p_{ij})_{I\times J}$ may be decomposed as:

$$\hat{P} = \hat{W}\hat{G}\hat{B} \tag{2}$$

The matrix $\hat{B}$=$(b_{ij})_{J\times J}$ is introduced to account for blurring, or spatial resolution, effects. It can be potentially used in modeling positron range, photon non-collinearity, the parallax effect as well as the radial/axial widths of the detecting crystals. It has been suggested [9] that image scatter may also be modeled by this blurring matrix.

The operator $\hat{G}$=$(g_{ij})_{I\times J}$ is subsequently utilized to geometrically forward-project all the voxel values along any desired line-of-response (LOR). The diagonal matrix $\hat{W}$=$(w_{ii})_{I\times I}$ allows a weight (e.g. attenuation and normalization) to be assigned to each LOR, to account for sensitivity variations.

Upon substituting the above expression for $\hat{P}$ into Eq. (1), and upon cancellation of $w_{ii}$ in the forward and back-projection steps, and using $\vec{S}$=$[s_1...s_J]^T$ and $\vec{\Lambda}^m$=$[\lambda_1^m...\lambda_J^m]^T$ to denote $J$-dimensional vectors of image sensitivity and image intensity (at iteration $m$), Eq. (1) can be written in the compact form [8]:

$$\vec{\Lambda}^{m+1} = \frac{\vec{\Lambda}^m}{\vec{S}} \times \hat{B}^T \left[ \sum_{k=1}^{N} \mathrm{BP}_{i_k} \left\{ \frac{1}{\mathrm{FP}_{i_k}(\hat{B}\vec{\Lambda}^m)} \right\} \right] \tag{3}$$

where vectorial multiplication and division operations are performed on an element-by-element basis, and $\mathrm{FP}_{i_k}$ and $\mathrm{BP}_{i_k}$ denote geometric operators which perform forward- and back-projection along LOR $i_k$ along which the $k$th list-mode event is detected.

We find it intuitively helpful to think of $\hat{B}$ as an operator that models the PSF response of the system by effectively blurring image intensities of all voxels into the neighboring voxels, which are then subsequently forward-projected. Upon application of the back-projection operation, the "deblurring" operation $\hat{B}^T$ is then invoked in order to position back-projected values from neighboring voxels back to the appropriate voxels.

In previous works, the spatial-blurring component $\hat{B}$ of the system matrix has been represented as a set of *space-invariant* and *isotropic* convolution kernels $\rho$ for ease of implementation. In this work, we have considered using the more appropriate generalization of having *position-dependent* and *anisotropic* kernel dimensions. Defining $\overrightarrow{R}$=$(X,Y,Z)$ as the position vector, each space-variant kernel $\rho(\overrightarrow{R})$ has been modeled as an anisotropic Gaussian, with the *distinct* widths ($\sigma_x(\overrightarrow{R})$, $\sigma_y(\overrightarrow{R})$, $\sigma_z(\overrightarrow{R})$) along the transaxial (X,Y) and axial (Z) directions dependent on *position-inside-FOV* of any voxel which is being blurred.

Various functional forms may be considered for the modeling of spatial distribution of the three kernel widths. We have considered exponential and inverse-Gaussian forms of degradation of image resolution, as given by

$$\sigma_i(\overrightarrow{R}) = \sigma_i(0) e^{\left(\frac{X}{L_{iX}}\right)} e^{\left(\frac{Y}{L_{iY}}\right)} e^{\left(\frac{Z}{L_{iZ}}\right)} \tag{4}$$

TABLE I

CHARACTERIZATION OF SPACE-VARIANCE AND ANISOTROPICITY

| | | | |
|---|---|---|---|
| $\sigma_x(0)$ | $L_{xX}$ | $L_{xY}$ | $L_{xZ}$ |
| $\sigma_y(0)$ | $L_{yX}$ | $L_{yY}$ | $L_{yZ}$ |
| $\sigma_z(0)$ | $L_{zX}$ | $L_{zY}$ | $L_{zZ}$ |

and

$$\sigma_i(\overrightarrow{R}) = \sigma_i(0) e^{\left(\frac{X^2}{2L_{iX}^2}\right)} e^{\left(\frac{Y^2}{2L_{iY}^2}\right)} e^{\left(\frac{Z^2}{2L_{iZ}^2}\right)} \tag{5}$$

where $i$=$x$, $y$ or $z$.

We therefore note that twelve parameters would be needed for this general parametrization of the blurring operator $\rho(\overrightarrow{R})$, as shown in table I. The horizontal extension of the table models XYZ-variant degradation of image resolution, and the vertical takes its anisotropicity into consideration.

## III. MEASUREMENT OF FINITE RESOLUTION KERNELS

In principle, object-independent components of blurring can be collectively modeled by scanning point sources positioned at various transaxial and axial positions in the FOV and reconstructing the scan data *without* any resolution modeling. The resulting spatial profiles can then be fit to yield the resolution kernel characteristic lengths. If it is desired to inherently include modeling of positron range, the point sources need to be inserted inside a medium of the same density as the regions in patients/animals in which emissions occur. Moreover, since magnitude of positron range depends on the positron energy, which varies widely among isotopes, such measurements will be isotope-specific. Modeling of image scatter would be more complex since it would have to take into consideration *size*, *type* and *structure* of object being scanned.

It must be noted that for the common case of 90°-transaxial-rotation symmetry (encountered, for instance, in circular or octagonal designs), it must be the case that

$$\sigma_x(0) = \sigma_y(0) \tag{6}$$

(i.e. (x/y)-resolution values at the center of the FOV are equal), and that the characteristic lengths satisfy

$$\begin{cases} L_{xX} = L_{yY} \\ L_{yX} = L_{xY} \\ L_{zX} = L_{zY} \end{cases} \tag{7}$$

by symmetry. These identities have been illustrated in Fig. (1).

It therefore follows that characteristic lengths obtained from the fitting of spatial distribution of resolution along one of the transaxial directions can be determined from the corresponding one in the other transaxial direction.

## IV. METHODS

*Tomograph:* Data were taken on the high resolution research tomograph (HRRT) [3]. This scanner has an octagonal design, with the detector heads consisting of a double 1 cm layer of

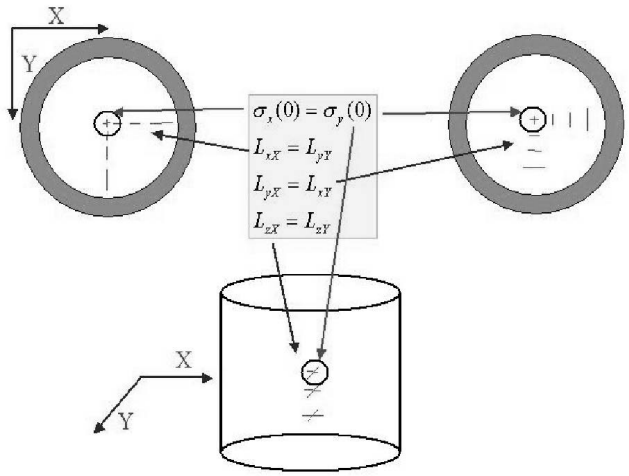


Fig. 1. Resolution relations implied by the common case of 90°-transaxial-rotation symmetry.

LSO/LYSO crystal layers for a total of 119,808 detector crystals (crystal size 2.1 x 2.1 x 10 $mm^3$). The total number of possible LORs is 4.486x$10^9$.

*Phantom used and measurement performed:* Four C-11 line sources, oriented axially, were *simultaneously* positioned in the horizontal (i.e. $Y$=0) direction of the transaxial plane by distances of $X$=0, 4, 8 and 12 cm from the center of the scanner. A scan duration of 7 minutes was considered resulting in 60.0M trues and 4.9M randoms. This study has been performed for the transaxial directions and is currently also being extended to the axial direction. Detector normalization correction factors were obtained from a 12 hour scan using a rotating rod source.

*Data analysis:* Ref. [10] should be consulted for details of implementation of the list-mode EM algorithm with random events correction on the HRRT. In this work, in order to determine variation of image resolution for the scanner, we have used the following technique: the simultaneously-scanned line-sources have been reconstructed by *space-invariant* and *isotropic* Gaussian kernels for a number of times with different $\sigma$ values ranging from 0 to 5 mm. Reconstructions were also performed using *space-variant* and *anisotropic* Gaussian kernels modeled with exponential as well as inverse-Gaussian forms of degradation of image resolution. Subsequently, transaxial widths ($w_x(X)$ and $w_y(X)$) of the four lines sources in the source were measured and compared (further elaborated in next section) at $X$=0,4,8,12 cm.

*Parallelization of Resolution Blurring* Parallelization of resolution blurring (along with list-mode reconstruction code was implemented on the University of British Columbia Dept. of Meteorology Linux Monster Cluster: a 128 x IBM eServers x330 with dual Pentium III: 1 GHz, 1 GB RAM, 256 KB cache system. The message passing interface (MPI) software was utilized to parallelize application of resolution blurring. The algorithm essentially consists of having several slave nodes perform spatial blurring on different regions of the image vector, results of which are passed to the master node for the overall image.

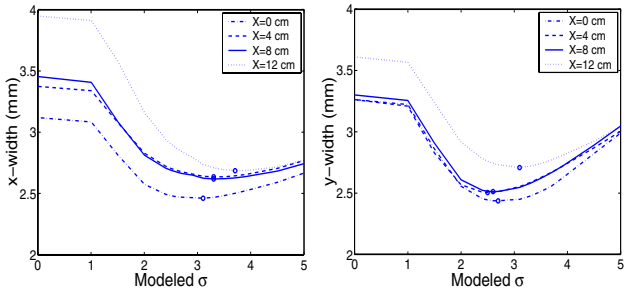


Fig. 2. Observed transaxial (x/y)-resolution values as functions of space-invariant, isotropic kernel $\sigma$ values. Points at which the curves are each minimized are indicated using circles.

## V. Results

*Space-invariant and isotropic resolution modeling:* Fig. (2) illustrates measured transaxial widths ($w_x(X)$ and $w_y(X)$) of the line sources as reconstructed for a wide range of Gaussian kernel widths. The following observations can be made:
(i) Improvement in reconstructed line widths upon performing space-invariant and isotropic modeling is significant compared to the case of performing no modeling whatsoever, i.e. ($\sigma_x$=$\sigma_y$=0).
(ii) For each imaged position, there exist unique intermediate modeling widths (referred to as $\widetilde{\sigma x}$ and $\widetilde{\sigma y}$) that minimize the reconstructed line widths. These points are marked using circles on each plot in the figure and are interpreted as modeling widths that best model PSF at the particular X-position.
(iii) $\widetilde{\sigma x}$ and $\widetilde{\sigma y}$ are not necessarily equal to one another for any imaged positions (anisotropicity).
(iv) Increasingly larger values of $\widetilde{\sigma x}$ and $\widetilde{\sigma y}$ are observed as one moves away from the center of the FOV (space-variance).

*Space-variant and anisotropic resolution modeling:* The spatial distribution of $\widetilde{\sigma x}$ and $\widetilde{\sigma y}$ (as obtained at X=0,4,8,12 cm) were then separately fit using exponential and inverse-Gaussian functions, from which values of $L_{xX}$ and $L_{yX}$ (and therefore $L_{yY}$ and $L_{xY}$ as given by symmetry Eqns. (7a) and (7b)) were determined. The resulting estimated characteristic lengths were then incorporated into the space-variant and anisotropic system matrix, and the data were subsequently reconstructed with the new system matrix.

For any reconstructed image, we have introduced an error measure:

$$\Delta = \frac{1}{N}\sum_i \sum_X \left[ \frac{(w_i(X) - w_i^{min}(X))}{w_i^{min}(X)} \times 100\% \right] \qquad (8)$$

where $i$=$(x, y)$, $X$=$(0, 4, 8, 12$ cm) (and therefore N=8 summations are performed), $w_i(X)$ indicates the line widths obtained using the particular modeling under consideration and $w_i^{min}(X)$ indicates the minimum width obtained using the procedure described in *data analysis* and illustrated in Fig. (2).

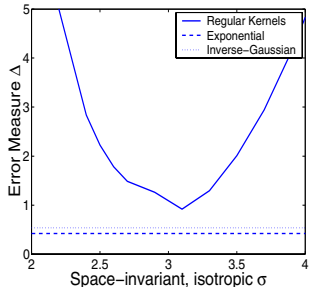


Fig. 3. Variation of $\Delta$ as a function of modeled space-invariant, isotropic $\sigma$ values, as described in text. Values achieved by using exponential and inverse-Gaussian modeling of degradation of resolution are also shown.

The above metric therefore measures the percentage difference between the reconstructed line widths and the *minimum* reconstructed line width, and averages it over the two transaxial directions and the four positions across the FOV. Value of $\Delta$ would therefore approach zero when a particular type of modeling achieves minimum observed widths *simultaneously* for *all* the lines across the FOV.

Fig. (3) plots $\Delta(\sigma)$ as a function of the various space-invariant, isotropic $\sigma$ values. The error measure has a minimum value of $\Delta$=0.914 obtained at $\sigma$=3.1 mm. By contrast, $\Delta$ values of 0.4169 and 0.5348 are obtained for exponential and inverse-Gaussian modeling of degradation of resolution across the FOV, as also shown in the figure. It is clearly seen that the latter error values are less than any $\Delta$ value obtained using regular modeling of $\sigma$ values.

## VI. Conclusion

In conclusion, we have shown that the introduction of a space variant and anisotropic point spread function (PSF), compared to a space-invariant and isotropic PSF, improves the resolution across the FOV. The spatial distribution of image resolution has been measured and fit using exponential and inverse-Gaussian profiles, from which twelve characteristic parameters were derived, and subsequently incorporated into the space-variant and anisotropic modeling of the system matrix.

We expect that future studies on scanners without DOI capability will better demonstrate the strengths of this approach. Further studies are intended also to select an accurate and optimum functional model, among many possible ones, of degradation of image resolution across the whole FOV for various scanners (with the possibility of utilizing look-up tables also considered). We also plan to characterize and model any existing skewness in the PSF away from the center of the FOV.

## Acknowledgments

This work was supported by the Canadian Institute of Health Research, the TRIUMF Life Science grant, the Natural Sciences and Engineering Research Council of Canada UFA (V.S.) and PGS B (A.R.) scholarships, as well as the Michael Smith Foundation for Health Research scholarship (V.S.).

## References

[1] P. R. G. Virador, W. W. Moses, and R. H. Huesman, "Reconstruction in PET Cameras with Irregular Sampling and Depth of Interaction Capability", *IEEE Trans. Nucl. Sci.* vol. 45, pp. 1225-1230, 1998.

[2] B. Karuta and R. Lecomte, "Effect of Detector Weighting Functions on the Point Spread Function of High-Resolution PET Tomographs: A Simulation Study", *IEEE Trans. Med. Imag.*, vol. 11, pp. 379-385, 1992.

[3] K. Wienhard, M. Shmand, M. E. Casey, K. Baker, J. Bao, L. Eriksson, W. F. Jones, C. Knoess, M. Lenox, M. Lercher, P. Luk, C. Michel, J. H. Reed, N. Richerzhagen, J. Treffert, S. Vollmar, J. W. Vollmar, J. W. Young, W. D. Heiss, and R. Nutt, "The ECAT HRRT: Performance and First Clinical Application of the New High Resolution Research Tomograph", *IEEE Trans. Nucl. Sci.* vol. 49, pp. 104-110, 2002.

[4] J. A. Fessler and S. D. Booth, "Conjugate-Gradient Preconditioning Methods for Shift-Variant PET Image Reconstruction", *IEEE Trans. Imag. Proc.*, vol. 8, pp. 688-699, 1999.

[5] J. W. Stayman and J. A. Fessler, "Compensation for Nonuniform Resolution using Penalized-Likelihood Reconstruction in Space-Variant Imaging Systems", To appear in *IEEE Trans. Med. Imag.*.

[6] A. J. Reader, P. J. Julyan, H. Williams, D. L. Hastings, and J. Zweit, "EM Algorithm Resolution Modeling by Image-Space Convolution for PET Reconstruction", *IEEE NSS & MIC 2002 conf. rec.*, Norfolk, VA, Nov 2002.

[7] L. Parra and H. H. Barrett, "List-mode Likelihood: EM algorithm and image quality estimation demostrated on 2-D PET", *IEEE Trans. Med. Imag.*, vol. 17, pp. 228-235, 1998.

[8] A. J. Reader, S. Ally, F. Bakatselos, R. Manavaki, R. Walledge, A.P. Jeavons, P.J.Julyan, S.Zhao, D. L. Hastings and J. Zweit, "One-Pass List-Mode EM Algorithm for High-Resolution 3-D PET Image Reconstruction Into Large Arrays", *IEEE Trans. Nucl. Sci.* vol. 49, pp. 693-699, 2002.

[9] R. Manavaki, A. J. Reader, C. Keller, J. Missimer and R. J. Walledge, "Scatter Modeling for 3-D PET List-Mode EM Reconstruction", *IEEE NSS & MIC 2002 conf. rec.*, Norfolk, VA, Nov 2002.

[10] A. Rahmim, M. Lenox, A. J. Reader, C. Michel, Z. Burbar, T. J. Ruth, and V. Sossi, "Weighted Iterative List-Mode Reconstruction for the High Resolution Research Tomograph", Proceed. of the VIIth Intern. Conf. on Fully 3D Reconst. in Radiol. and Nucl. Med. (Mo PM3-2), Saint-Malo, France (2003)